Tip Vortex/Airfoil Interaction for a Low Reynolds Number Canard/Wing Configuration

F. A. Khan*
Boeing Commercial Airplane Company, Seattle, Washington 98124
and
T. J. Mueller†
University of Notre Dame, Notre Dame, Indiana 46556

The effects of the vortical wake shed by a finite span canard on a low Reynolds number airfoil were examined. Aerodynamic performance was evaluated through direct measurements of lift, drag, and 1/4-chord pitching moment. Spanwise static pressure and surface film visualization data were also acquired. A reduction in the downstream airfoil drag coefficient and an increase in its lift/drag were noted in the presence of the canard for a wide range of configurations. Static pressure and surface visualization data provided indication of some of the boundary-layer characteristics responsible for the drag behavior.

Nomenclature

A_W = wing area
b = wing semispan
C_D = wing drag coefficient, $D/(A_W q_\infty)$
C_L = wing lift coefficient, $= L/(A_W q_\infty)$
C_M = wing moment coefficient, $= M/(cA_W q_\infty)$
C_P = static pressure coefficient, $= (P-P_\infty)/q_\infty$
c = wing chord length
c_c = canard chord length
D = wing drag force
L = wing lift force
M = wing 1/4-chord pitching moment
O_c = canard offset, Z_c/c
P = static pressure
q = dynamic pressure, $= 1/2(\rho U^2)$
R_c = chord Reynolds number, $= cU_\infty/V$
S = nondimensional separation distance, $= X_c/c$
U_∞ = freestream velocity
X_c = streamwise distance between canard/wind 1/4-chord axes
x = chordwise coordinate
y = spanwise coordinate
Z_c = vertical displacement of canard 1/4-chord axis with respect to wing 1/4-chord axis
a = wing incidence
a_c = canard incidence
δ_c = declage, $= (a_c - \alpha)$
ϵ = downwash angle
ν = kinematic viscosity
ρ = density

Introduction

THE emergence, in recent years, of small remotely piloted vehicles (mini RPVs) for military and scientific use has created a demand for low Reynolds number ($R_c < 10^6$) aerodynamic data. In this regime, the transition of the boundary layer on airfoils is characterized by the formation of a laminar separation bubble. A simplified sketch of a laminar separation bubble (or simply, a bubble) is shown in Fig. 1. For low chord Reynolds numbers, the airfoil boundary layer remains laminar past the point of maximum suction. An adverse pressure gradient of sufficient magnitude can cause the laminar boundary layer to separate from the airfoil surface. The separated shear layer may undergo transition and, due to the entrainment of energetic fluid, reattach as a turbulent boundary layer. The region bounded by the shear layer and the airfoil surface, between the points of separation and reattachment, is the laminar separation bubble. The prediction of bubble size and location is pivotal to low Reynolds number airfoil and wing design because it is associated with the transition of the boundary layer. The presence of a bubble can also adversely affect the airfoil static pressure distribution. The reader is directed to Refs. 1-3 for a more complete treatment of low Reynolds number airfoil aerodynamics.

In addition to understanding the behavior of simple two-dimensional airfoils, the effective design of mini RPVs requires aerodynamic performance data for more complex configurations at low Reynolds numbers. A substantial amount of research has been conducted at the University of Notre Dame to address this need. References 4-6 are typical examples.

The present work examines the effects of the vortical wake shed by a finite span canard on a low Reynolds number airfoil. The parameters used to describe the relative geometry of the wing and canard are shown in Fig. 2. The offset O_c is the nondimensional vertical spacing between the canard and wing 1/4-chord axes. It is positive when the canard is situated above the

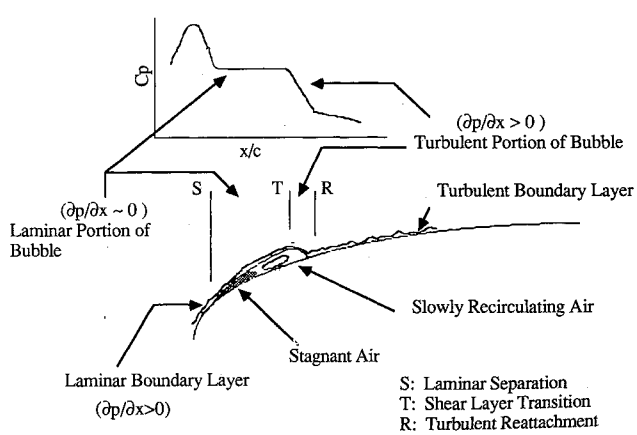

Fig. 1 Simplified sketch of a laminar separation bubble.

Presented as Paper 89-0536 at the AIAA 27th Aerospace Sciences Meeting, Reno, NV, Jan. 9-12, 1989; received April 18, 1989; revision received June 1, 1990; accepted for publication June 19, 1990.

*Engineer. Member AIAA.

†Roth-Gibson Professor, Department of Aerospace and Mechanical Engineering. Associate Fellow AIAA.

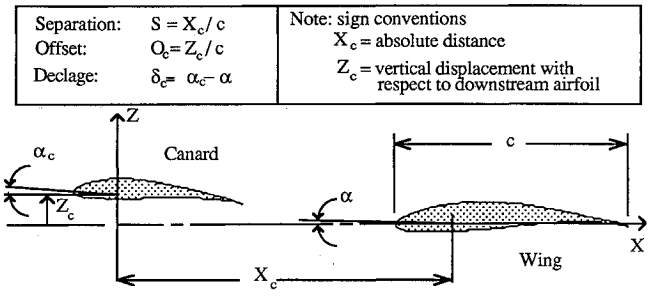

Fig. 2 Geometric parameters.

Table 1 Wind tunnel models

Model	Span, cm	Chord, cm
Semispan canard model (wooden construction)	28	10
Wing model used for force/moment measurements and flow visualization (cast epoxy construction)	40	15
Modular model for spanwise static pressure measurements (cast epoxy construction)	40	15

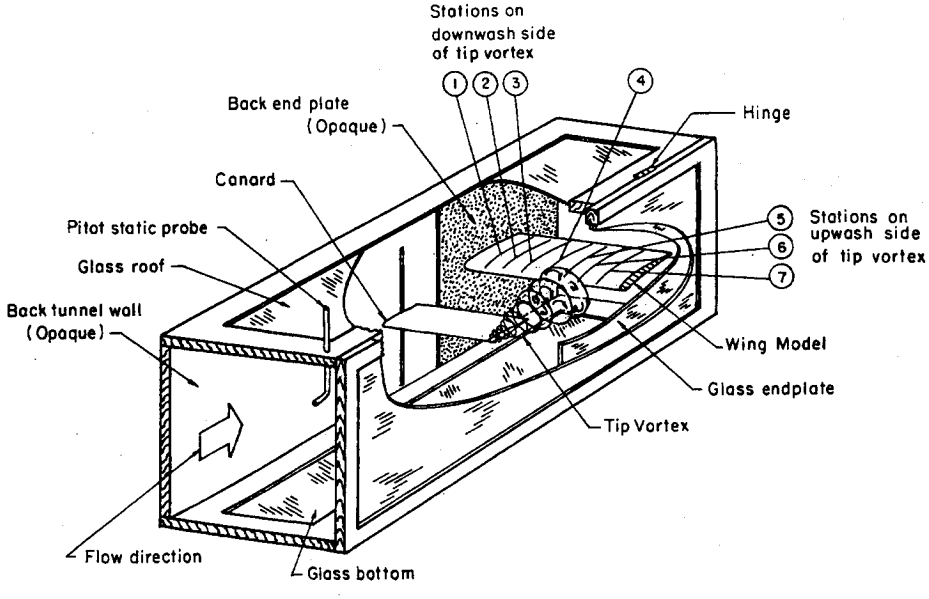

Fig. 3 Test section used for static pressure measurements and flow visualization.

wing and negative when the canard is below the wing. The nondimensional horizontal separation S is always a positive number and is also measured from the respective 1/4-chord locations. The declage δ_c is the incidence of the canard relative to the wing.

The interaction of the downstream airfoil with the canard tip vortex and wake was studied by varying the vertical position of the wake with respect to the wing, i.e., by changing O_c. Lift, drag, and 1/4-chord pitching moment (LDM) data were acquired in order to evaluate the aerodynamic performance of the downstream airfoil. The prominent features of the airfoil boundary layer were examined by means of spanwise static pressure measurements. The latter was helpful in locating regions of separated flow on the airfoil. The tip vortex/airfoil interaction was visualized using a kerosene vapor tracer.

The downstream airfoil will be referred to as the "wing" throughout the following discussion. The aerodynamic performance coefficients for the wing in the presence of the canard will be denoted by uppercase subscripts, e.g., C_L. Coefficients for the wing without the canard will be denoted by the additional subscript "SA," e.g., $(C_L)_{SA}$. This nomenclature reflects the aim of the aerodynamic performance measurements, namely, to isolate the effects of the canard vortical wake on the performance of a three-dimensional wing.

Apparatus

All models used during the present study were of rectangular planform with Wortmann FX 63-137 profiles. The coordinates of this airfoil section are given in Ref. 4. The three models used for the various experiments are described in Table 1. The canard model was of wooden construction and had a semispan aspect ratio of 2.8. The modular pressure model was comprised of four spanwise sections. These could be arranged seven different ways, with each configuration yielding a differenct spanwise location for the chordwise array of pressure taps. The pressure tap stations are illustrated in Fig. 3. Details of the design and construction of the pressure model are given in Ref. 7.

The experiments were conducted in the South subsonic wind tunnel of the Aerospace Laboratory at Notre Dame. The tunnel is an open circuit, atmospheric exhaust design. The working section is 183 cm long and has a square cross section of 61 cm on the side. Turbulence intensity (U_{rms}/U_{mean}) in the working section is 0.08% for the 1-2500 Hz bandwidth.[8]

LDM data on the wing were measured using an external platform balance. Both the wing and canard were mounted vertically from the tunnel ceiling. Each was supported at its 1/4-chord axis. A gap of 3 mm was maintained between the ceiling and the inboard end of the canard. The gap was large enough to allow the canard to be rotated through its entire range of incidences and at the same time preclude the formation of a tip vortex at the inboard end. A traversing mechanism mounted on the tunnel roof allowed the canard to be positioned at various offset locations. The wing was flanked at either end by end plates. These shielded it from the tunnel-wall boundary layer and, more important, minimized the spanwise variation of aerodynamic loads concomitant with a finite aspect ratio. A distance of 7 cm separated the upper end plate from the ceiling. A tare shroud prevented the portion of the wing support between the upper end plate and tunnel ceiling from contributing to the aerodynamic loads measured by the balance. Tunnel dynamic pressure was monitored by means of a pitot static probe located near the test section/inlet juncture.

During the static pressure test, the models were mounted horizontally, in cantilever fashion; see Fig. 3. The relative geometry of the canard and wing was the same as that for the

LDM measurements described earlier. A Scanivalve switch wafer served as a multiplexer, allowing the pressure taps to be sampled sequentially.

Visualization of the tip vortex/airfoil interaction was conducted using kerosene vapor as tracer and stroboscopic illumination. A form of surface film visualization was used to supplement the static pressure data. Propylene Glycol with a small smount of Fluorescein was smeared on the wing. The resulting flow patterns were viewed under ultraviolet light and recorded on black and white film. The basic technique is described in Ref. 9.

Results

In order to identify changes in wing performance due to the finite span canard, data were acquired on the wing with and without the canard. The latter represents the baseline configuration. Throughout the following discussion, data corresponding to the wing in the absence of the canard will be referred to as "single airfoil data." All data are uncorrected for solid body blockage, wake blockage, and wall interference effects. The lack of detailed knowledge about the flowfield and the number of configurations studied made the use of simple tunnel corrections (such as those suggested in Ref. 9) of suspect value. The blockage due to the canard and wing was, however, estimated using the methods of Ref. 9 and was found to be negligibly small. The dynamic pressure was adjusted for streamwise buoyance due to the growth of the boundary-layer displacement thickness along the tunnel walls. This was done by measuring the difference between the dynamic pressure at the test section/inlet juncture and the wing model location prior to data acquisition. The difference was then factored into the dynamic pressure computions during data acquisition.

Figures 4 show the performance coefficients as a function of angle of attack for the wing in baseline configuration at $R_c = 150{,}000$. LDM data for the wing in tandem with the canard were acquired at wind incidences of 0, 5, and 10 deg. For each wing incidence, positive declages of 0, 2.5, and 5 deg were studied. The offset was varied from -0.5 to $+0.5$ in increments of 0.033. Only the $\alpha = 0$ and 10 deg cases are presented here. A discussion of the wing performance at $\alpha = 5$ deg may be found in Ref. 7. All results for the wing in tandem with the canard correspond to a separation distance $S = 3$ and a value of $R_c = 150{,}000$.

Wing Incidence: 0 Deg

Overlay plots of the wing lift coefficient as a function of canard offset for $\alpha = 0$ deg and positive declages of 0, 2.5, and 5.0 deg are shown in Fig. 5a. The plots are characterized by three distinct regions. The first is a flat "plateau" on the extreme left. A "bucket" forms the second and central region. A second plateau to the right of the bucket forms the third region. The single airfoil lift coefficient $(C_L)_{SA}$ is indicated by the horizontal line. The performance of the wing is influenced by the change in effective angle of attack (downwash) due to the bound and shed vorticity of the canard and by the relative position of the canard wake. Between $O_c = -0.5$ and -0.2, the wing C_L remains within 1.5% of the single airfoil value. This represents the range of offsets for which the canard wake is below the wing and downwash effects are negligible. Beyond $O_c = -0.2$, the downwash and the effects of the momentum deficient wake become manifest. The lift coefficient declines until a minimum is reached. The offsets corresponding to the minima vary with declage, as does the value of $(C_L)_{\min}$. As declage increases, the minimum shifts to more positive offsets. For $\alpha_c = 0$ deg, $(C_L)_{\min} = 0.637$ [4.5% lower than $(C_L)_{SA}$] occurs at $O_c = 0.067$; for $\alpha_c = 2.5$ deg, $(C_L)_{\min} = 0.637$ [4.5% below $(C_L)_{SA}$] is reached at $O_c = 0.1$; whereas for $\alpha_c = 5.0$ deg, a minimum lift coefficient of 0.641 [4.3% below $(C_L)_{SA}$] occurs at $O_c = 0.167$.

As noted earlier, the bucket in Fig. 5a is a consequence of the net reduction in the effective angle of attack due to the bound and shed vorticity of the canard and the momentum deficient wake shed by it. The bound vorticity is that which creates the circulation about a lifting surface (in the present case, the canard); the shed vorticity is concentrated in the tip vortex. The spanwise location of the canard tip approximately coincides with the wing midspan ($0.5b$). Therefore, roughly equal portions of the wing experience downwash and upwash from the canard tip vortex. The bound vorticity of the canard, however, predominantly affects the inboard half of the wing (i.e., the portion of the wing that lies on the downwash side of the tip vortex). Thus, the reduction in the effective angle of attack on the inboard half outweighs the effect of the upwash on

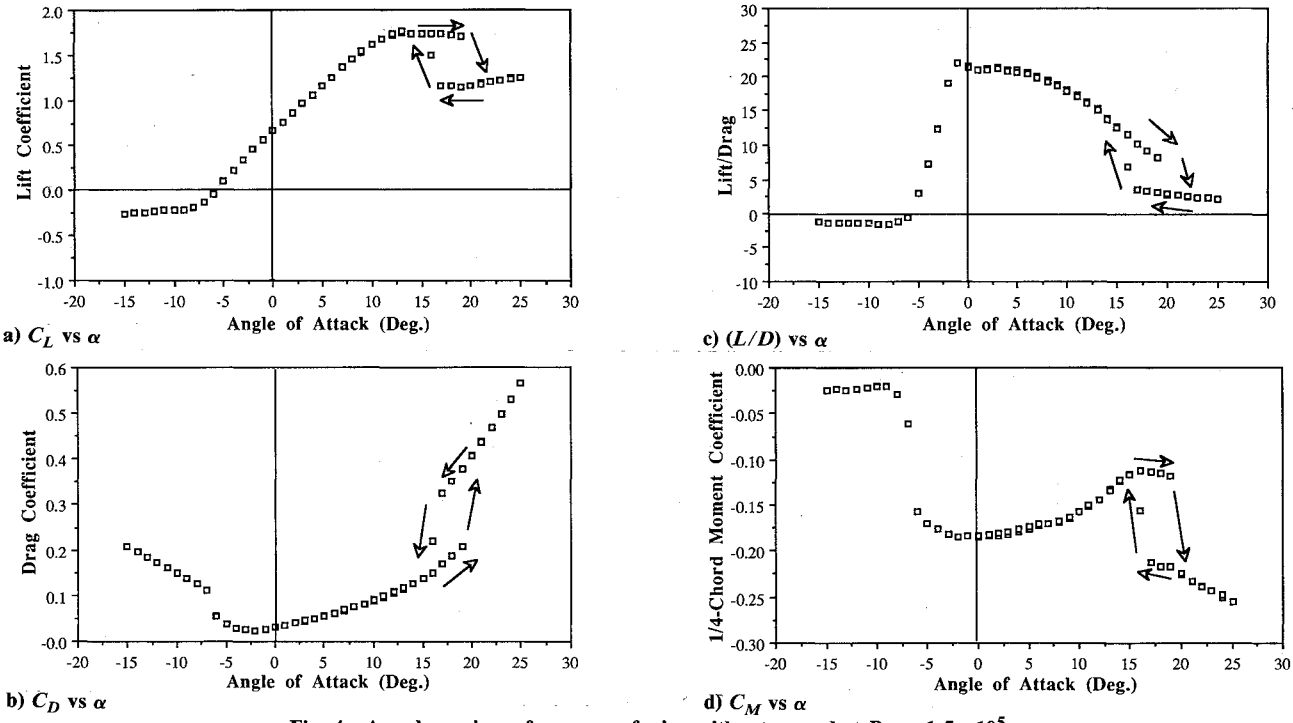

Fig. 4 Aerodynamic performance of wing without canard at $R_c = 1.5 \times 10^5$.

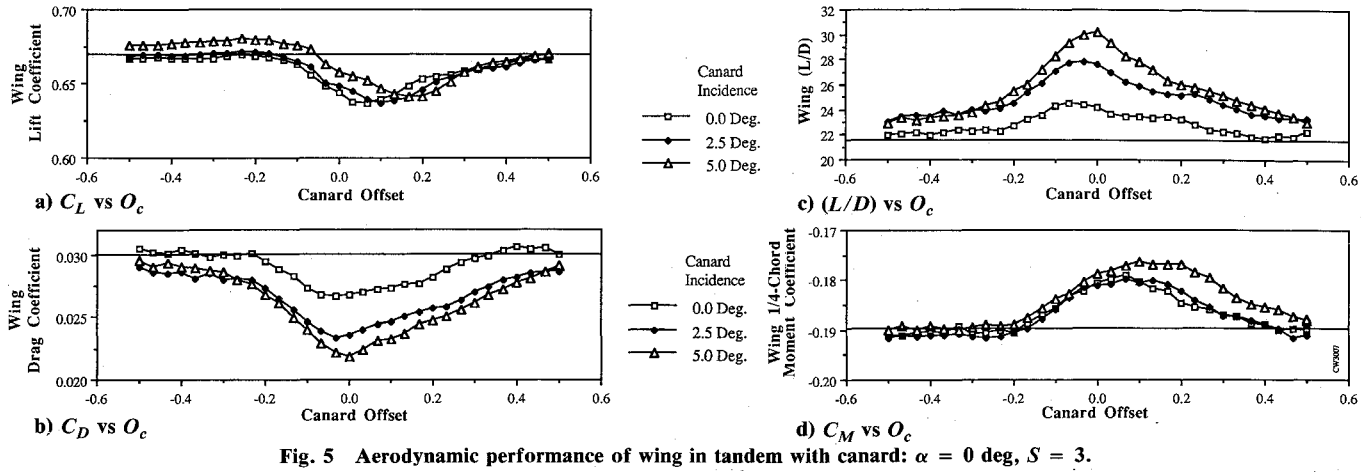

Fig. 5 Aerodynamic performance of wing in tandem with canard: α = 0 deg, S = 3.

the outboard portion of the wing. The result in a net decrement in the mean incidence and, hence, C_L for the wing. This is true for all offset and separation configurations.

The magnitude of the downwash (or upwash) is also dependent on the distance between the wing and canard. From potential flow theory, the bound vorticity of any two-dimensional wing section may be localized at the 1/4-chord point. The downwash angle (i.e., the net change in the angle of attack induced by the airfoil section) is approximately given by

$$\epsilon = \arctan[C_l/(4\pi r')]$$

The term r' is the nondimensional distance $(c/c_r)\sqrt{(S^2+O_c^2)}$. For a constant S, the quantity (O_c^2/r') decreases as the magnitude of the offset increases. This implies that for a given section lift coefficient ϵ at a point on the wing is highest for $O_c = 0$ and diminishes as the canard approaches the extremities of the offset range. In a similar way, the induced angle of attack due to the tip vortex (the swirl angle) varies directly with the proximity of the vortex core to the wing. This is a somewhat simplistic view because the bound and shed vorticity vary along the span of the canard. Moreover, the tip vortex does not become fully developed until some distance downstream of the canard trailing edge. These discrepancies notwithstanding, the explanation serves as a heuristic device.

The arguments presented so far do not account for the canard wake. Because of its finite thickness, the wake acts to modify the direction of the streamlines in the inviscid flowfield. The streamlines above the wake are deflected so as to reduce the downwash imposed by the canard. Similarly, deflection of the inviscid flow streamlines below the wake increases the downwash in that region. The existence of a well-defined plateau to the left of the bucket and the absence of one on the right (Fig. 5a), supports this hypothesis. The effect of the momentum deficit in the canard wake is to reduce the magnitude of the aerodynamic loads experienced by the wing. When these reduced loads are nondimensionalized using the dynamic pressure of the undisturbed stream ahead of the canard, the resulting coefficients are smaller in magnitude.

Figure 5b is an overlay plot of C_D vs offset for α = 0 deg and positive declages of 0, 2.5, and 5 deg. As in the case of the C_L plot discussed earlier, the curves in Fig. 5b display three regions: a well-defined plateau for extreme negative offsets, a bucket region for middle offsets, and a second (less well-defined) plateau on the positive end of the offset range. The curve corresponding to α_c = 0 deg shows the three regions with the greatest clarity. The first plateau extends from $O_c = -0.5$ to -0.2 (same as for the curves in Fig. 5a). A minimum drag coefficient of $(C_D)_{\min} = 0.027$ occurs at $O_c = -0.33$: a 10% drop from the single airfoil drag coefficient. The bucket region ends at approximately $O_c = 0.3$ with C_D approaching the single airfoil value of 0.03 (indicated by the horizontal line). A minimum drag coefficient of 0.023 is reached at $O_c = -0.033$ for α_c = 2.5 deg [21% below $(C_D)_{SA}$]. For α_c = 5 deg, $(C_D)_{\min} = 0.022$ [24% lower than $(C_D)_{SA}$] occurs at $O_c = 0$. For the two higher declages, a plateau region at positive offsets is almost nonexistent. The two curves do, however, approach the single airfoil drag coefficient.

In order to understand the C_D behavior in Fig. 5b, it should be noted that the wake impingement on the wing has a dual effect on the drag. The slower velocities in the wake reduce the magnitude of the drag force. Nondimensionalization of the reduced drag force with the undisturbed freestream dynamic pressure gives a lower C_D. However, the higher turbulence intensities in the wake are likely to hasten transition on portions of the wing. The resulting increase in skin friction drag would work to offset the reduction in C_D due to the downwash and momentum deficient wake.

Comparison of Figs. 5a and 5b reveals two major differences between the lift and drag behavior. First, the offsets corresponding to $(C_D)_{\min}$ and $(C_L)_{\min}$, for a given declage, are not coincident. Second, the percent reduction in drag is much greater than that in C_L. These two factors combine to yield values of (C_L/C_D) that are substantially better than $(C_L/C_D)_{SA}$. Figure 5c shows overlay plots of (C_L/C_D) vs O_c for α = 0 deg and positive declages of 0, 2.5, and 5 deg. The single airfoil value of $(C_L/C_D) = 21.5$ is indicated by the horizontal line. Values of $(C_L/C_D)_{\max}$ for α_c = 0, 2.5, and 5 deg cases are 14, 29, and 40% higher than $(C_L/C_D)_{SA}$, respectively.

The variation of the wing 1/4-chord pitching moment with O_c at α = 0 deg and δ_c = 0, 2.5, and 5 deg is shown in Fig. 5d. The range of offsets for which the magnitude of C_M falls below the single airfoil value corresponds closely to the bucket region in the C_L plot [Fig. 5a and with the high (C_L/C_D) values Fig 5c]. A less negative C_M might be beneficial in a canard-wing configuration since it reduces the overall nose-down pitching moment contribution of the wing. As a consequence, smaller canard angles would be required to trim a vehicle employing such a configuration. In short, the trim drag at or near the $(C_L/C_D)_{\max}$ point would be lower. Maximum reduction in C_M is about 5–7%.

As noted earlier, the maximum improvement in (C_L/C_D) occurs for α = 0 deg, α_ϕ = 5, and $O_c = 0$. Static pressure and surface film visualization results for this configuration are summarized in Figs. 6. In the absence of the canard, a bubble exists on the upper and lower surfaces of the wing. Over the inboard half of the wing ($y < 0.5b$), the downwash due to the canard shifts the upper surface bubble downstream, while the upwash over the outboard half ($y > 0.5b$) causes an upstream shift in the upper surface bubble. On the lower surface, the bubble is completely absent on the inboard half indicating that the flow remains laminar throughout. This is believed to contribute significantly to the improvement in (C_L/C_D). The secondary flow near the inboard end on the upper surface is due to the velvet on the inboard end plate. The black velvet was used to enhance contrast between the gray-white smoke

and the background during flow visualization. The glass end plate at the outboard end did not produce any significant end effects. The impingement of the canard tip vortex on the wing caused a sharp rise in the upper surface suction near the leading edge and a region of secondary flow along $y = 0.5b$. Figure 7 shows smoke flow visualization of the interaction.

Wing Incidence: 10 Deg

Fig. 8a shows overlay plots of C_L vs O_c for $\alpha = 10$ deg and canard incidences of 10, 12.5, and 15 deg. All three curves merge and approach the single airfoil lift coefficient of 1.6 at the far negative offsets. The values of C_L approached at the positive end of the offset range fall short of the single airfoil lift coefficient. The discrepancey is a small one, about 3% at worst. The canard influences the wing over a wider range of offsets than for $\alpha = 0$ deg. In the present case, the bound vorticity of the canard is stronger and the wake wider, resulting in a reduction in C_L over a wider range of offsets. The bound vorticity of the canard also imposes a downward velocity on the wake. The minima experienced by the C_L curves near $O_c = 0$ are the result of the strong downwash. At higher offsets, the canard wake begins to interact with the wing preventing the recovery of C_L to its single airfoil value.

The wing C_D as a function of offset for canard incidences of 10, 12.5, and 15 deg and $\alpha = 10$ deg is shown in Fig. 8b. The disparity between the percent decrease in the value of C_L and C_D is not as significant as for $\alpha = 0$ deg. As a result, the (C_L/C_D) values show relatively modest improvements over the single airfoil case. Maximum gains in (C_L/C_D) of 6, 11, and 13%, respectively, are noted for declages of 0, 5, and 10 deg in Fig. 8c.

Spanwise static pressure measurements and surface film visualization provide some insight into the (C_L/C_D) behavior. A sketch of the regions of separated flow on the wing upper surface for $\alpha = 10$ deg, $\alpha_c = 15$ deg, and $O_c = -0.167$ is shown in Fig. 9. This configuration corresponds to the maximum (C_L/C_D) in Fig 8c. The upwash on the outboard half ($y > 0.5b$) causes the bubble to diminish in its chordwise extent and shift toward the leading edge. This is accompanied by turbulent separation near the trailing edge. The downwash on the inboard portion of the wing ($y > 0.5b$) has the opposite effect, leading to an increase in the laminar flow. The reduction in drag over the inboard half outweighs the adverse effects experienced by the outboard portion yielding a net increase in (C_L/C_D). No evidence of vortex impingement on the upper surface was suggested by the pressure measurements of the surface film visualization. Flow visualization of the tip vortex/wing interaction Fig. 10 shows that the vortex trajectory does in fact lie below the wing.

The sketch in Fig. 11 depicts the wing upper surface for $\alpha = 10$ deg, $\alpha_c = 15$ deg, and $O_c = 0$. The (C_L/C_D) in Fig. 8c is sharply reduced for this configuration. The flow on the outboard half of the wing is predominantly turbulent. Turbulent separation occurs farther upstream than for $O_c = -0.167$. As seen in Fig. 12, the vortex impacts the upper surface near the leading edge. The proximity of the vortex core causes strong suction near the leading edge and a secondary flow region around $y = 0.5b$ on the upper surface. The net effect of the strong upwash and the vortex interaction is an increase in C_D and reduction in (C_L/C_D) to a value below the single airfoil case (Fig. 8c).

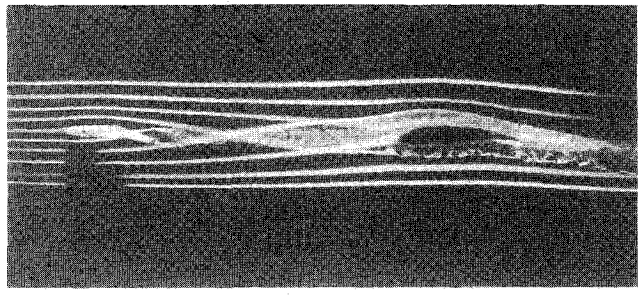

Fig. 7 Visualization of tip vortex/airfoil interaction: $\alpha = 0$ deg, $\alpha_c = 5$ deg, $O_c = 0$, and $S = 3$.

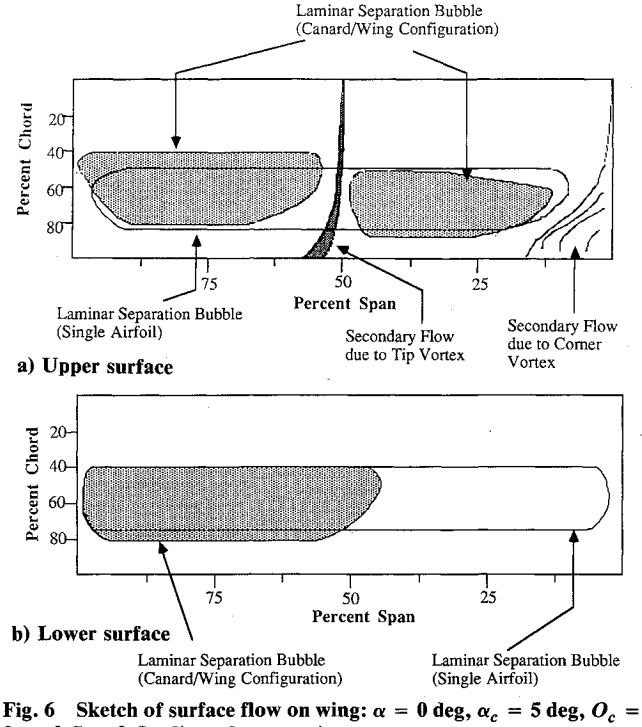

Fig. 6 Sketch of surface flow on wing: $\alpha = 0$ deg, $\alpha_c = 5$ deg, $O_c = 0$, and $S = 3$ (leading edge at top).

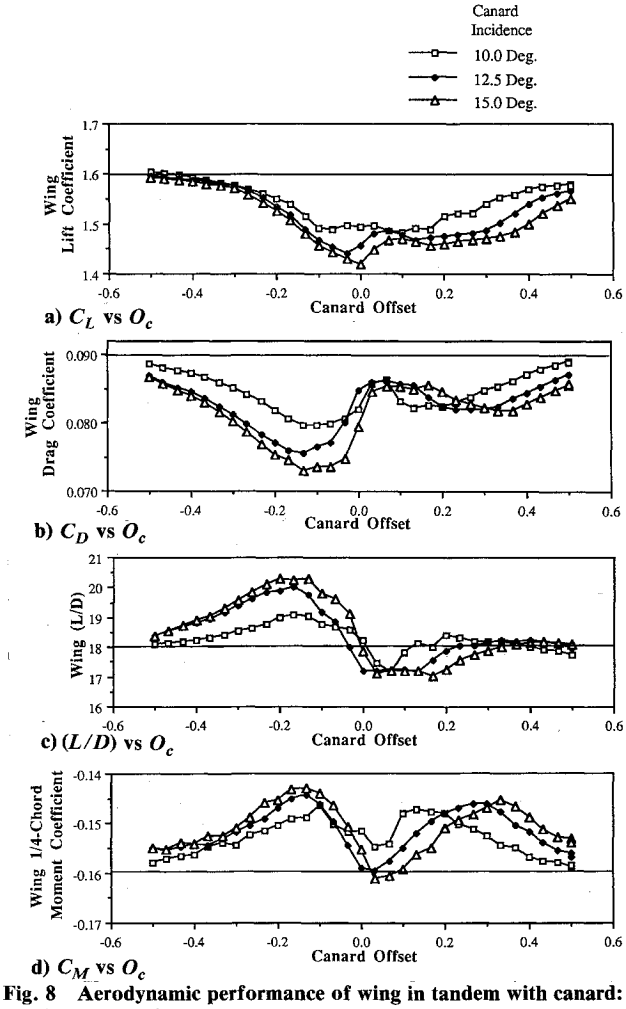

Fig. 8 Aerodynamic performance of wing in tandem with canard: $\alpha = 10$ deg, $S = 3$.

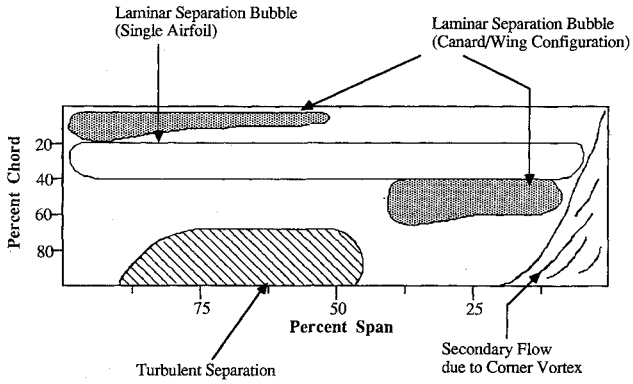

Fig. 9 Sketch of upper surface flow on wing: α = 10 deg, α_c = 15 deg, O_c = −0.167, and S = 3 (leading edge at top).

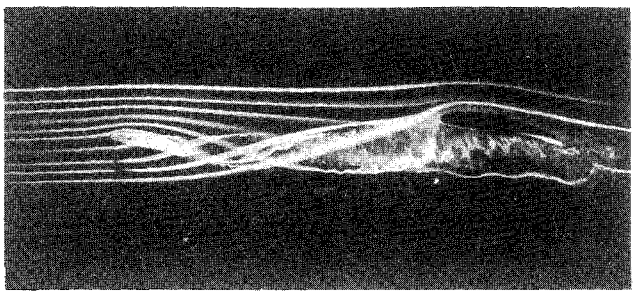

Fig. 10 Visualization of tip vortex/airfoil interaction: α = 10 deg, α_c = 15 deg, O_c = −0.167, and S = 3.

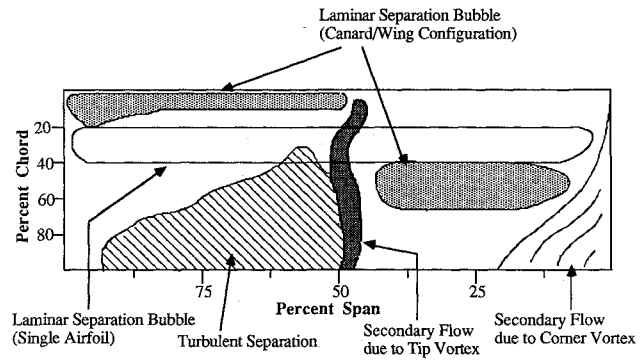

Fig. 11 Sketch of upper surface flow on wing: α = 10 deg, α_c = 15 deg, O_c = 0, and S = 3 (leading edge at top).

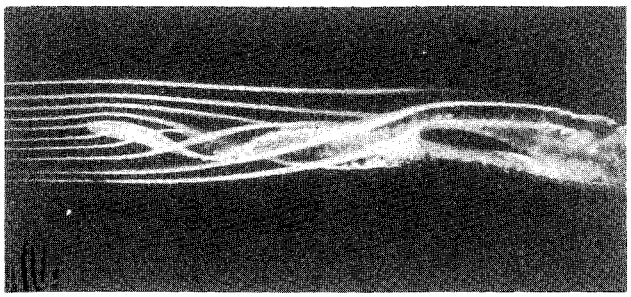

Fig. 12 Visualization of tip vortex/airfoil interaction: α = 10 deg, α_c = 15 deg, O_c = 0, and S = 3.

Concluding Remarks

The position of the tip vortex and wake shed by the canard profoundly influences the performance of the wing. The magnitude of the aerodynamic loads is reduced when the momentum deficient wake impinges directly on the wing. The non-dimensional force and moment coefficients, based on the undisturbed freestream dynamic pressure, are also lowered as a consequence. The net downwash imposed by the canard acts to further reduce the magnitudes of the coefficients.

Due to the streamline curvature introduced by the canard wake, the downwash is stronger below the wake than above it. Hence, of two canard locations an equal distance above and below the offset corresponding to $(C_L)_{\min}$, the wing C_L is higher for the more negative offset. The value of $(C_L)_{\min}$ decreases as declage increases. This is caused by the stronger downwash and a greater momentum deficit in the wake associated with higher canard incidences.

For all wing incidences studied, C_D is below the corresponding single airfoil value over a wide range of offsets. Futher, the reduction in C_D is much more drastic than that in C_L. As a consequence, the wing (C_L/C_D) is higher than the single airfoil lift/drag ratio. The most significant improvements occur at α = 0 deg where the wing $(C_L/C_D)_{\max}$ is up to 40% higher than $(C_L/C_D)_{SA}$. The range of offsets at which (C_L/C_D) is the highest is also the one over which C_D is minimum and C_M is least negative. The reduction in the magnitude of C_M promises savings in trim drag since smaller canard deflections will be needed to offset the destabilizing (nose-down) moment due to the wing.

The behavior of the aerodynamic coefficients for α = 0 deg described earlier formed a trend and was also observed at α = 10 deg. However, it was noted that the reduction in C_D and the increase in (C_L/C_D) is not as significant at the higher wing incidence.

The identification of boundary-layer characteristics through the use of static pressure measurements and surface film visualization was helpful in understanding some of the factors responsible for the C_D behavior. In general, the bubble is shifted downstream over the inboard portion of the wing due to the canard downwash. The reduction in skin friction drag due to this delayed transition acts to lower the C_D. Similarly, the upwash at the outboard portion of the wing causes an early transition of the boundary layer. At higher wing incidences and positive declages, turbulent separation at the outboard stations adds to the overall drag. The savings in C_D due to the reduction in skin friction drag over the inboard half of the wing erodes as a consequence of the last two factors.

Acknowledgments

The research reported in this paper was supported by the Department of Navy, Office of Naval Research under Contract N00014-83-K-0239 and by the Department of Aerospace and Mechanical Engineering, University of Notre Dame.

References

[1]Tani, I., "Low Reynolds Number Flows Involving Bubble Separations," *Progress in Aeronautical Sciences,* Vol. 5, pp. 77–103.

[2]Lissaman, P. B. S., "Low Reynolds Number Airfoils, *Annual Review of Fluid Mechanics*, Vol. 15, 1983, pp. 223–239.

[3]Mueller, T. J., "Low Reynolds Number Vehicles," edited by E. Reshotko, AGARDograph No. 288, 1985.

[4]Bastedo, W. G., Jr., and Mueller, T. J., " Spanwise Variation of Laminar Separation Bubbles at Low Reynolds Numbers," *Journal of Aircraft,* Vol. 23, No. 9, 1986, pp. 687–694.

[5]Perry, M. L., and Mueller, T. J., "Leading- and Trailing-Edge Flaps on a Low Reynolds Number Airfoil," *Journal of Aircraft,* Vol. 24, No. 9, 1987, pp. 653–659.

[6]Michelsen, W. D., and Mueller, T. J., "Low Reynolds Number Airfoil Performance Subjected to Wake Interference From an Upstream Airfoil," AIAA Paper 87-2351, Aug. 1987.

[7]Khan, F. A., "The Performance of a Low Reynolds Number Airfoil in Tandem with a Finite Span Canard," M. S. Thesis, University of Notre Dame, Notre Dame, IN, Jan. 1989.

[8]Brendel, M., and Mueller, T. J., "Boundary-Layer Measurements on an Airfoil at Low Reynolds Numbers," *Journal of Aircraft,* Vol. 25, No. 7, 1988, pp. 612–617.

[9]Rae, W. H., and Pope, A., *Low Speed Wind Tunnel Testing,* 2nd ed., Wiley, New York, 1984.